SAND2017-13379C

Effects of Cavity Width on Resonance Dynamics using Time-Resolved PIV and PSP

Justin L. Wagner,[1] Steven J. Beresh,[2] Katya M. Casper[3], Edward P. DeMauro,[4*] Kyle P. Lynch,[5] Russell W. Spillers,[6] John F. Henfling,[7] Seth M. Spitzer,[8]

Sandia National Laboratories, Albuquerque, NM, 87185

The spanwise variation of resonance dynamics in the Mach 0.94 flow over a finite-span cavity of variable length-to-width ratio was explored. Time-resolved particle image velocimetry (TR-PIV) in a planform plane above the cavity and time-resolved pressure sensitive paint (TR-PSP) on the adjacent wind tunnel walls around the cavity were used to investigate the dynamics. The PIV showed a significant variation in resonance dynamics to occur across the span of the cavity. This spanwise variation was a strong function of the cavity aspect ratio and was only weakly dependent on the cavity mode number. A substantial influence of the sidewalls appears to arise from spillage vortices stemming from finite-width effects. PSDs of streamwise velocity in the region of the spillage vortices showed a large peak to occur at modes one through three, indicating that resonance dynamics, and not just broadband turbulence effects, are prevalent near the sidewalls. Large peaks in modal pressures were also present just outside of the cavity. Interestingly, prominent peaks at the mode frequencies were observed in the spanwise velocity spectra as well. Collectively, the observed three-dimensional resonance dynamics in a finite-span cavity motivate the need to move understanding beyond the classical two-dimensional Rossiter mechanism.

I. Introduction

Cavity flow is an analog to flow over an aircraft bay. As such, the topic has garnered much attention over the last sixty-plus years as described in multiple review articles [1-4]. The flow over an open cavity generates large pressure fluctuations associated with turbulence and cavity resonance [5]. In subsonic flows, when the cavity length-to-depth ratio L/D is less than about seven [6], a resonant feedback loop occurs with an interaction of the cavity's acoustic field and the cavity shear layer. The resonant modes are thought to be primarily longitudinal and in simple rectangular geometries, the tonal frequencies are reasonably predicted by the semi-empirical relation provided by Rossiter [5].

The spatial distribution of modal resonance fluctuations throughout the cavity flow field is paramount to understanding the response of internal structures such as stores [7-9] as well as store separation [10]. Unfortunately, in comparison to modal frequencies, the prediction of the modal amplitudes is much more difficult. The spatial resonance distributions are known to be sensitive functions of the flow conditions and the cavity geometry, although analytical functional forms for these effects are lacking. Three-dimensional effects are important. For instance,

[1] Principal Member of the Technical Staff, Engineering Sciences Center, P.O. Box 5800, Mailstop 0825; jwagner@sandia.gov. AIAA Senior Member.
[2] Distinguished Member of the Technical Staff, Engineering Sciences Center, AIAA Associate Fellow.
[3] Senior Member of the Technical Staff, Engineering Sciences Center, AIAA Senior Member.
[4] Post-doctoral Appointee, Engineering Sciences Center, AIAA Senior Member, *Currently Assistant Professor, Rutgers University.
[5] Post-doctoral Appointee, Engineering Sciences Center, AIAA Member.
[6] Principal Technologist, Engineering Sciences Center.
[7] Distinguished Technologist, Engineering Sciences Center.
[8] Technologist, Engineering Sciences Center, AIAA Senior Member.

Sandia National Laboratories is a multi-mission laboratory managed and operated by National Technology and Engineering Solutions of Sandia, LLC., a wholly owned subsidiary of Honeywell International, Inc., for the U.S. Department of Energy's National Nuclear Security Administration under contract DE-NA0003525.

several studies have shown that changes to the length-to-width ratio L/W ratio can significantly change the resonance amplitudes [6, 11-14]. Moreover, geometric complexities such as inflow ramps and doors can alter and enhance resonance tones [15-17].

Cavity dynamics involve complex interactions of the mixing layer, recirculating flow, turbulence, and acoustic waves. A given cavity flow is typically associated with several tonal frequencies and the modal amplitudes are modulated in time [18-22]. A common, quantitative consensus on the physical mechanisms of cavity tone modulations, and the relationship between resonance pressure fluctuations and cavity flow field dynamics in general, has yet to be achieved.

To elucidate dynamics in compressible cavity flows, recent work by the current authors has sought to measure spatial distributions of resonance using a combination of time-resolved particle image velocimetry (TR-PIV) and time-resolved pressure sensitive paint (TR-PSP) [23-25]. Consistent with the Rossiter mechanism [5], TR-PSP on the cavity floor has shown modal surface pressures to exhibit streamwise periodicity generated by the interference of downstream-traveling disturbances in shear layer with upstream-traveling acoustical waves [23]. Accompanying TR-PIV data, acquired along the spanwise center plane, have also shown clear evidence of this interference through the modulation of coherent flow structure. With analogy to a standing wave, the modal velocity fields were found to contain local maxima at locations containing pressure minima and vice-versa [25].

Despite recent progress on understanding spatial distributions of resonance in the flow-field, little work has focused on how resonance dynamics vary across the span of the cavity. Since resonance amplitudes are known to be a function of L/W [6, 11-14], it is not clear how the interference patterns observed in the flow-field at the cavity center [25] will vary as the sidewalls are approached. If the cavity has finite-span, the cavity sidewalls can result in creation of spillage vortices, which can introduce streamwise vorticity into the flow-field [17, 26-32]. Previous work by the present authors in the supersonic [30] and transonic [31] regimes has shown elevated turbulence levels near the sidewalls associated with inflow into the cavity and (i.e., spillage vortices).

In the present paper, the variation of resonance dynamics across the cavity span are investigated. TR-PIV data taken in a planform plane above the cavity lip-line are reported for aspect ratios of $L/W = 1$, $L/W = 1.67$ and $L/W = 5$. Additionally, TR-PSP data are presented both along the cavity floor as well as on the wind tunnel floor adjacent to the cavity cutout. Experiments were performed at a single Mach number of 0.94 where resonance is strong at the first three cavity tone frequencies. These measurements allow the spatial variation in resonance dynamics associated with spillage vortices and cavity walls to be evaluated.

II. Experimental Program

A. Trisonic Wind Tunnel (TWT)

Experiments were conducted in the blowdown-to-atmosphere TWT. The facility uses air as the test gas and has a test section enclosed in a pressurized plenum. Data were obtained at a freestream Mach number M_∞ of 0.94 (U_∞ = 311 m/s), which was determined using a freestream velocity measurement at the cavity entrance location [25] and the assumption of isentropic expansion. Thirty wind tunnel runs were made at each cavity geometry. Typical flow conditions for the experiments conducted in the 305 × 305 mm^2 test section are given in Table 1. The tunnel wall boundary layers developed naturally and were fully turbulent upon arrival at the test section. Previous measurements have indicated that the 99% wall boundary layer thickness at the cavity entrance is about 13 mm or about half the cavity depth. The boundary layer momentum and displacement thicknesses were roughly 1.4 mm and 1.7 mm, respectively.

Table 1: Typical TWT Experimental Conditions

M_∞	P_0, kPa	T_0, K	Re × 10^{-6}, /m
0.94	60	321	13

In subsonic cavity flows it is necessary to mitigate the undesirable acoustical interference associated with solid wind tunnel walls by placing an acoustic absorber in the wall opposite to the cavity [18, 33-34]. The spanwise walls of subsonic test sections can also lead to acoustical contamination if untreated [35]. To reduce these effects, the wall opposite the cavity and one spanwise wall were replaced with acoustic dampeners. The dampeners consisted of a porous wall, used typically for transonic testing, backed by acoustical absorption foam. A modification of the porous wall was made to allow a small laser exit window to pass the outgoing planform aligned PIV laser sheet. The

opposite spanwise wall was solid with a window providing a view for the PIV cameras and access for incoming laser sheet.

B. Cavity Hardware

The cavity had a length L of 127 mm and depth D of 25.4 mm and was installed in the lower wall of the test section in experiments using PIV (Fig. 1a). Three different cavity widths W of 127 mm, 76.2 mm, and 25.4 mm were investigated to access the effects of width on resonance distributions. The cavities are hereafter referenced using the ratio of cavity length to width (i.e. 5 × 5, 5 × 3, and 5 × 1). In separate experiments using TR-PSP, the cavity was instead installed in the ceiling of the wind tunnel and the cavity floor was viewed through windows in the lower walls of the test section and plenum (Fig. 1b). At an L/D of 5, the cavity flow is expected to resonate [6]. The streamwise (x), wall-normal (y), spanwise (z) coordinate system originates at the spanwise center of the cavity leading edge (Fig. 1a). The wind tunnel floor is defined to be at $y = 0$, with positive y pointing away from cavity.

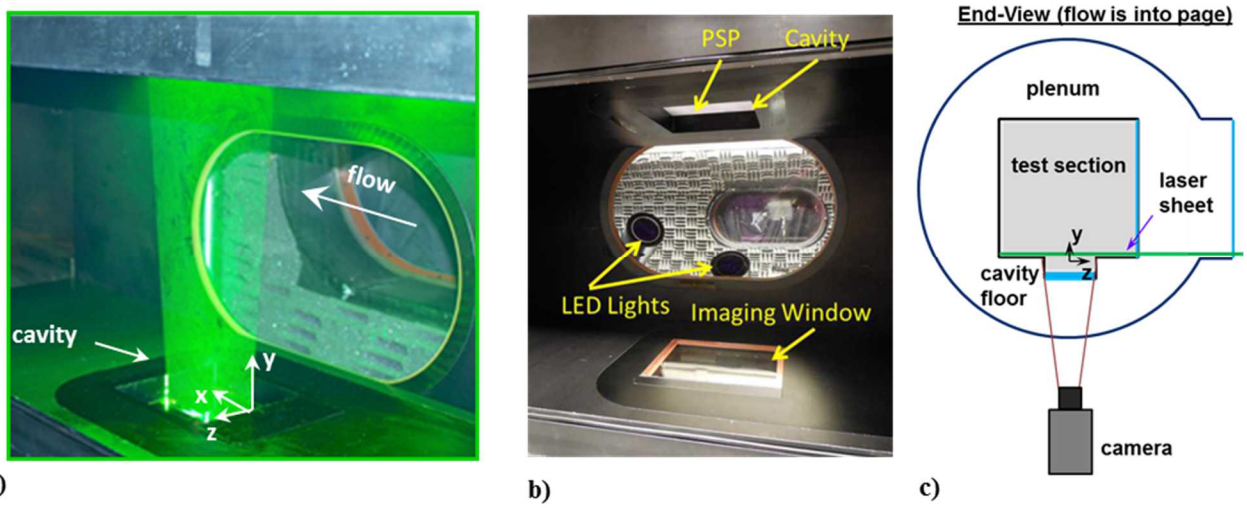

Fig. 1 Experimental details: a) Photo of cavity in the lower wall of the test section. The photo is from previous experiments where the laser sheet was brought in through a cavity floor window, b) photo of cavity installed in the upper test section wall for PSP experiments, and c) schematic of TR-PIV setup.

C. Unsteady Pressures

Dynamic pressure sensors (Kulite XCQ-062-30A) having a range of about 207 kPa and a flat frequency response up until about 50 kHz were placed in the cavity fore wall ($x = 0$) and the cavity aft wall ($x = 5D$). The sensors were located at $z = 0$. The sampling frequency was 200 kHz and the data were lowpass-filtered at 50 kHz.

High-frequency PSP from Innovative Scientific Solutions, Inc. (ISSI) was sprayed onto the entire floor of the cavity (Fig. 1b). In addition, although not shown in the figure, PSP was painted on the wind tunnel in regions adjacent to the cavity. The paint used a platinum-tetra-fluoro-phenyl-porphyrin (PtTFPP) luminophore added on top of a porous ceramic binder. The porosity of the base layer added surface area to allow fast response of the paint. Specifically, a frequency response of approximately 10 kHz was possible making it essentially time-resolved for resonance dynamics characterized herein. Moreover, importantly, the paint measurements have been shown to be in good agreement with pressure sensors [23].

Three ISSI LM2XX-DM-400 water-cooled light arrays excited the PSP over a range of about 400 nm ± 30 nm. The lights were placed in the plenum surrounding the tunnel to locate them as close as possible to the cavity. Most of the emission from the paint was centered at a wavelength near 650 nm. A high-speed camera (Photron SA-Z) fitted with a 50-mm lens was used to acquire full-view images of the cavity at framing rates of 20 kHz. The camera had a resolution of 1024 x 1024 pixels and a quantum efficiency of 49% at 630 nm. A 590 nm long-pass filter removed the 400-nm excitation light.

Raw images were post-processed using an adaptive Wiener filter in Matlab. This acted as a low-pass filter to reduce additive noise in the images. Static calibrations were used to convert the intensity ratios to pressure ratios, yielding the unsteady pressure fluctuations within the cavity. Additional details on the calibration and TR-PSP setup can be found in Casper et al. [23].

D. Time-Resolved Particle Image Velocimetry

Seeding was provided by a smoke generator that delivered a large quantity of mineral oil particles to the tunnel stagnation chamber. Measurement of the particle response across a shock wave has shown the particle size to be about 0.8 μm, which returns Stokes numbers of about 0.04 based on *a posteriori* measurements of typical cavity shear layer eddies. The particles, therefore, rapidly attain the local velocity even in the presence of velocity gradients in the shear layer [36]. Visual inspection of the PIV images showed adequate seeding in all portions of the cavity, including the recirculation region.

A quasi-continuous burst-mode laser (QuasiModo-1000, Spectral Energies, LLC) with both diode and flashlamp Nd:YAG amplifiers was used to produce a high energy pulse train at a wavelength of 532 nm. The laser design is based on a master oscillator power amplifier architecture and is like previously reported pulse-burst lasers [37-38]. As detailed in [39], the laser can produce doublets with the variable inter-pulse spacing time and at varying pulse frequencies (repetition rates). Here, the laser was operated at 25 kHz with doublets separated in time by 6 μs. A 10.2 ms burst was generated every 8 seconds and the energy per pulse was about 40 mJ. Five bursts per wind tunnel run brought the total number of bursts to 150. The beam was shaped into a laser sheet covering the entire span of the cavity. The laser sheet had a wall-normal thickness of 2.0 mm, and was located at the location of $y = 0.13D$.

Images were acquired using a high-speed camera (Photron SA-Z) operated at 50 kHz at a resolution of 640 × 592 pixels. The camera looked through the floor of the cavity made of a glass window. The two pulses in a doublet were frame-straddled around the inter-frame transfer time of the cameras to produce separate images for cross-correlation analysis. As a result, the PIV repetition rate was half that of the framing-rate, or 25 kHz. The final vector field encompassed a streamwise by spanwise region of roughly 100 × 125 mm ($4D \times 5D$).

The image pairs were processed using the LaVision PIV software package DaVis v8.4 to a final interrogation window size of 32 × 32 pixels at an overlap of 75% using three passes in total. The resulting vector fields were validated based upon signal-to-noise ratio, nearest-neighbor comparisons, and allowable velocity range. The final spatial resolution was 1.3 mm

E. Analysis Methods

Power spectral densities of the pressure and velocity data were computed in Matlab using the Welch windowing algorithm (*pwelch* function). A window overlap of 50% was used. PSDs based on the pressure sensor data utilized a window length Δf of 20 Hz, whereas the window lengths in the TR-PSP and TR-PIV PSDs were 50 Hz and 100 Hz, respectively.

For the velocity data, the square root of the PSD is reported, which is normalized by the freestream velocity U_∞ to yield units of $Hz^{-0.5}$. In the case of the pressure data, frequency spectra are reported in decibels as sound pressure level SPL:

$$\mathrm{SPL}(f) = 10\log_{10}\left[\frac{\mathrm{PSD}_p(f)\Delta f_{ref}}{p_{ref}^2}\right] \quad (1)$$

where PSD_p represents the power spectral density of pressure, p_{ref} is a reference pressure set to the standard 20 μPa, and Δf_{ref} is a reference frequency set here to 1 Hz. Spatial distributions of the PSD amplitude at frequencies corresponding to cavity tones are shown herein to highlight the spatial variation associated with resonance in both the pressure (TR-PSP) and velocity (TR-PIV) fields. The TR-PSP fields are based on a single run lasting 0.5 seconds (10,000 samples), whereas the TR-PIV PSDs are averages of the 150 independent bursts.

III. Results

A. Aft Wall Pressure Spectra

SPL spectra obtained at the aft wall sensor for all three cavity geometries are shown in Fig. 2. The cavity modes are denoted M in the figure. Like several studies [6, 11-14], these spectra demonstrate a dependence of resonance on the cavity width. The modal frequencies corresponding to the 5 × 5 and 5 × 3 cavities are within 2% of the values predicted using the modified Rossiter relation of Heller and Bliss [40]. On the other hand, the 5 × 1 cavity exhibits frequencies that are 100-200 Hz lower than the wider cavities at each of the first modes (M1 – M4). Modes one through three have relatively equal amplitude in the 5 × 5 geometry, whereas mode one has the greatest amplitude in the 5 × 3 geometry spectrum. The most striking difference between the three geometries occurs at the first modal frequency of the 5 × 1 cavity where M1 exhibits diminished amplitude in comparison to the wider cavities. Notably,

previous measurements at Mach numbers ranging from 0.6 – 1.5 also show a strong mode one in the 5 × 5 and 5 × 3 cavities and a weak mode one amplitude in the 5 × 1 geometry [14].

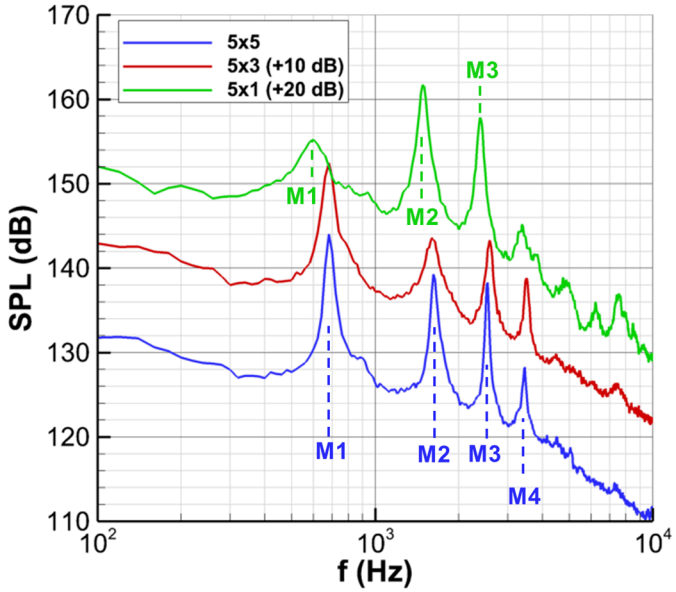

Fig. 2 SPL spectra at the aft wall of the cavity. The 5 × 3 and 5 × 1 spectra are offset for clarity.

B. Mean and Turbulence Fields

Contours of the mean streamwise velocity component U in the plane above the cavity ($y = 0.13D$) are shown in Fig. 3 for each cavity configuration. The walls of the cavity are depicted with gray rectangles. In each configuration, the streamwise velocity decreases with increasing streamwise distance as the mixing layer grows in thickness. In the case of the 5 × 5 and 5 × 3 cavities, a marked decrease in U occurs near the sidewalls beginning at $x = D$. In contrast, the 5 × 5 cavity exhibits a much smaller decrease in streamwise velocity near the sidewalls with some spillage occurring near the aft end.

The contours of mean spanwise velocity W shown in Fig. 4 tell a similar story. Flow into the cavity is observed at $x > 3D$ with the effects of the sidewalls more pronounced in the two wider cavities. Previous stereoscopic measurements, which revealed the out-of-plane component of velocity V, suggest the spillage to be associated streamwise aligned vorticities [41]. The additional undulations in spanwise velocity near the spanwise center of the 5 × 3 cavity likely suggest the presence of a counter rotating vortex pair. This observation is consistent with DeMauro et al. [17] who identified a counter rotating vortex pair near the spanwise center of an $L / W = 2$ cavity using volumetric reconstruction of planar PIV data. The 5 × 1 cavity, on the other hand, is apparently not wide enough to support additional vortex pairs, whereas, the 5 × 5 cavity contains W variations consistent with a total of three vortex pairs. These undoubtedly oversimplified explanations are summarized in the illustrative cartoons below each contour plot.

Contours of streamwise turbulence intensity are displayed in Fig. 5. The influence of spillage near the sidewalls results in significantly elevated turbulence intensities in the two wider cavities. Like the Mach 0.8 10-Hz PIV measurements of Beresh et al. [31], the narrowest cavity has decreased turbulence levels near the sidewalls. Spanwise turbulence levels are given Fig. 6, where substantially increased fluctuation levels are observed near the sidewalls in the 5 × 5 and 5 × 3 cavities. One difference with respect to the streamwise turbulence plots is that peak spanwise fluctuations occur at a more inboard location. Like the mean flow fields, undulations in turbulence levels are observed over the span of the cavity.

The dependence of turbulence levels on location is captured further in the spanwise line profiles of Fig. 7. As annotated with the rectangles in Fig. 5a, the turbulence levels were averaged over x to produce upstream ($x < 3D$) and downstream ($x < 4D$) profiles. This analysis was performed for each cavity configuration on both components of turbulence intensity.

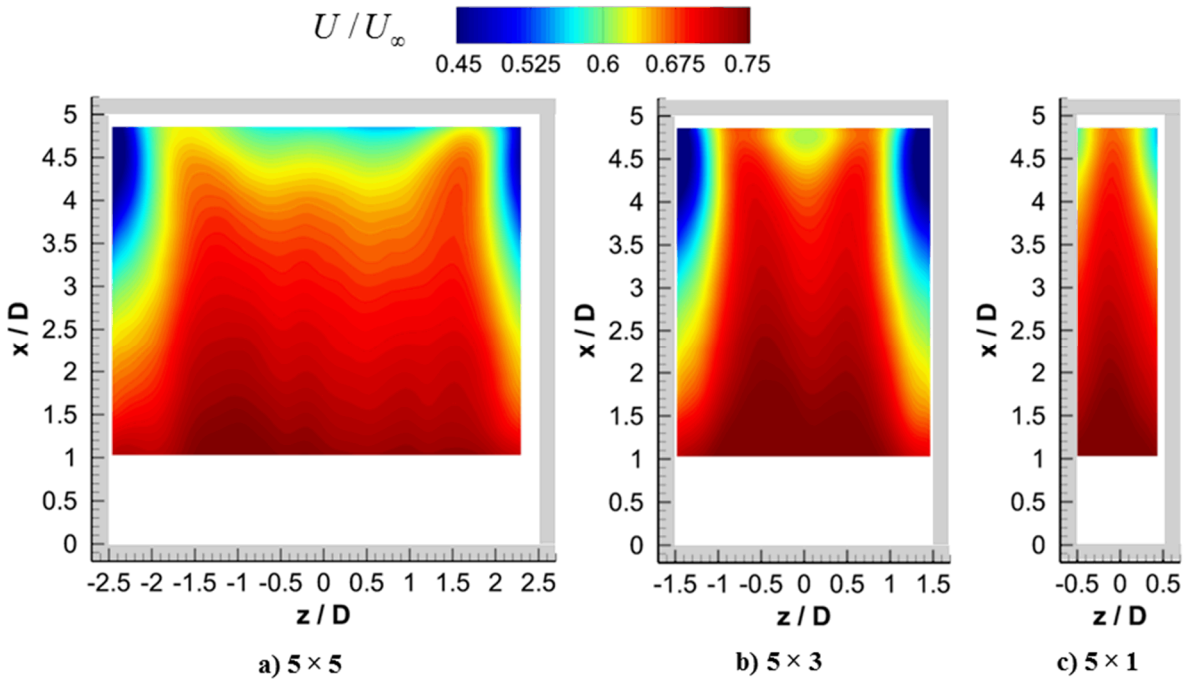

Fig. 3 Mean streamwise velocities normalized by U_∞. Flow is from bottom-to-top.

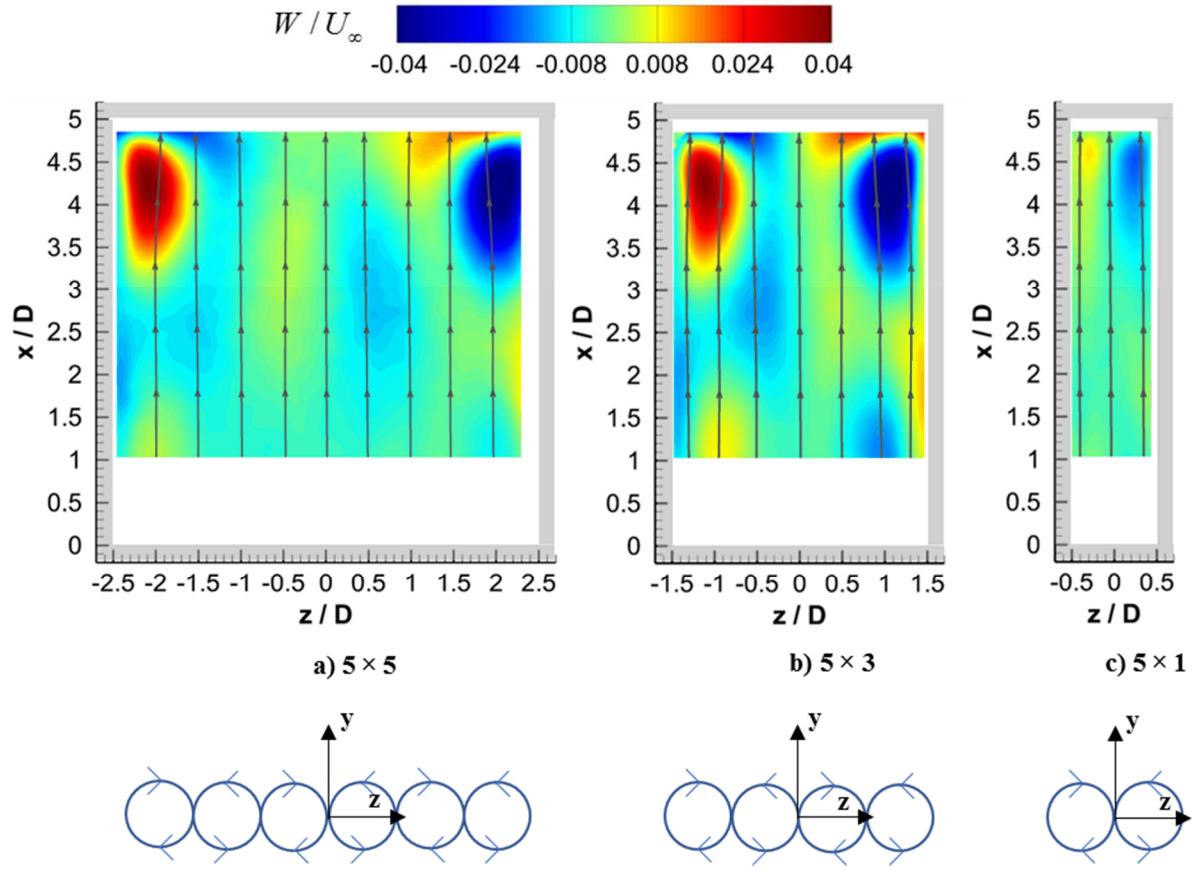

Fig. 4 Mean spanwise velocities normalized by U_∞ with overlaid streamlines (top) and simplified cartoon depicting hypothesized streamwise aligned vortices (bottom) where flow is into the page.

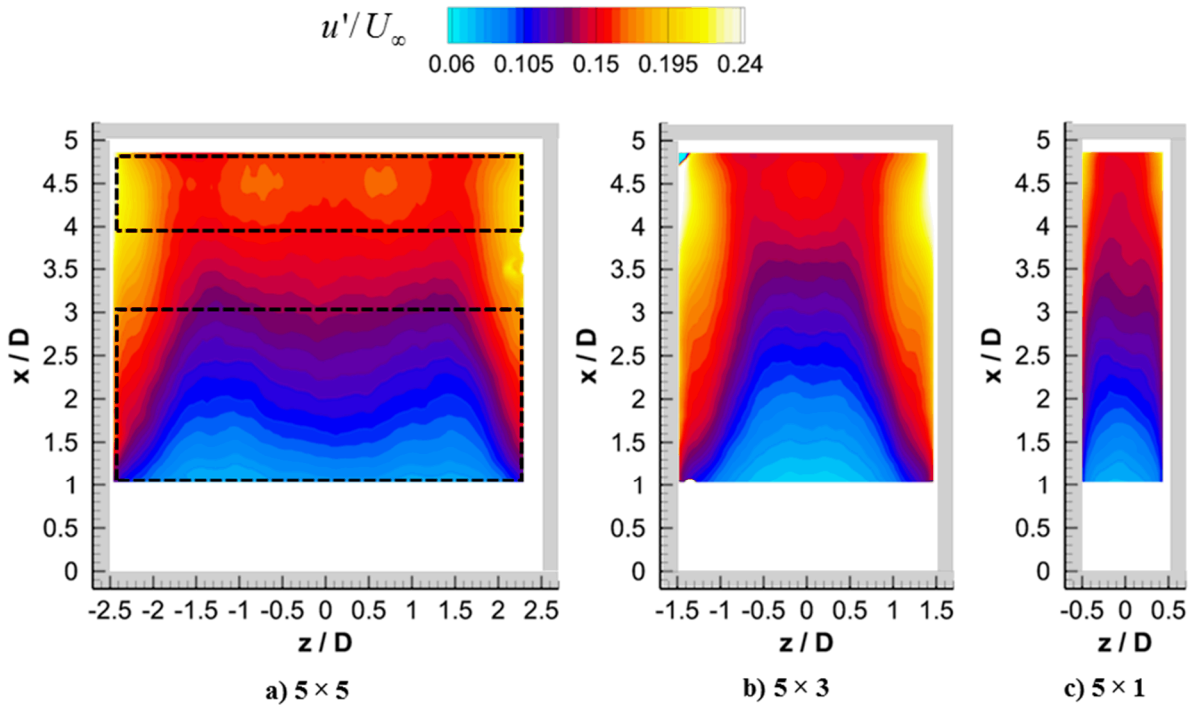

Fig. 5 Contours of streamwise turbulence intensity. Dashed, black rectangles indicate the regions over which spanwise profiles were produced for subsequent figures.

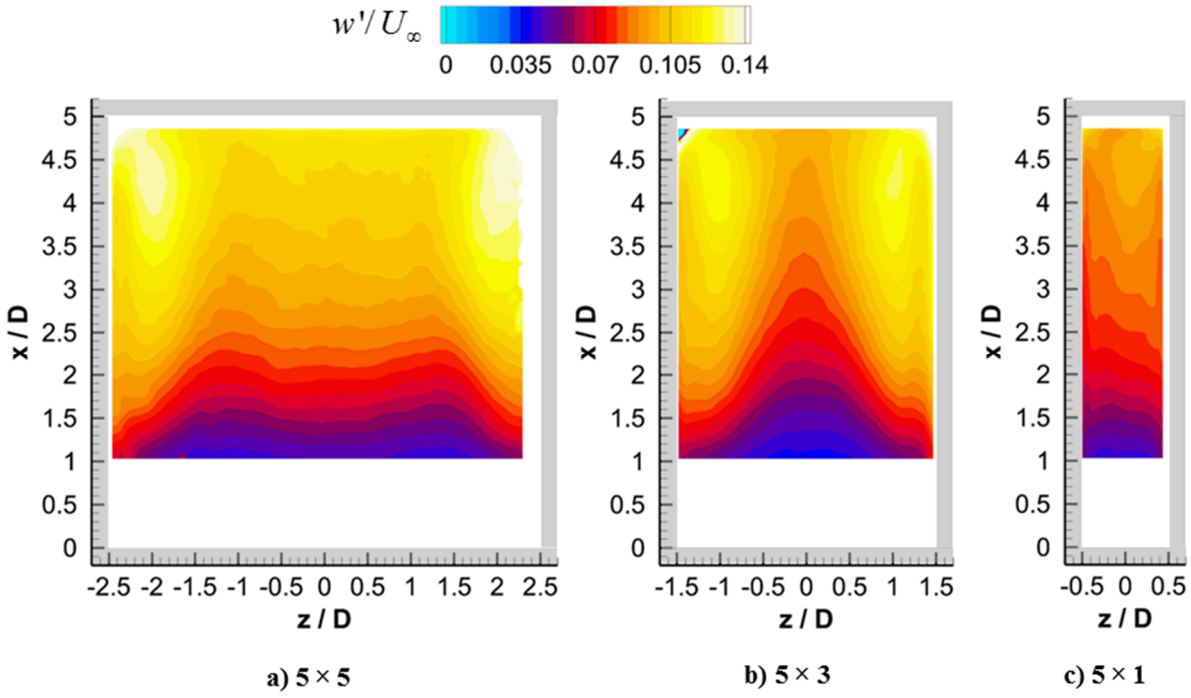

Fig. 6 Contours of spanwise turbulence intensity.

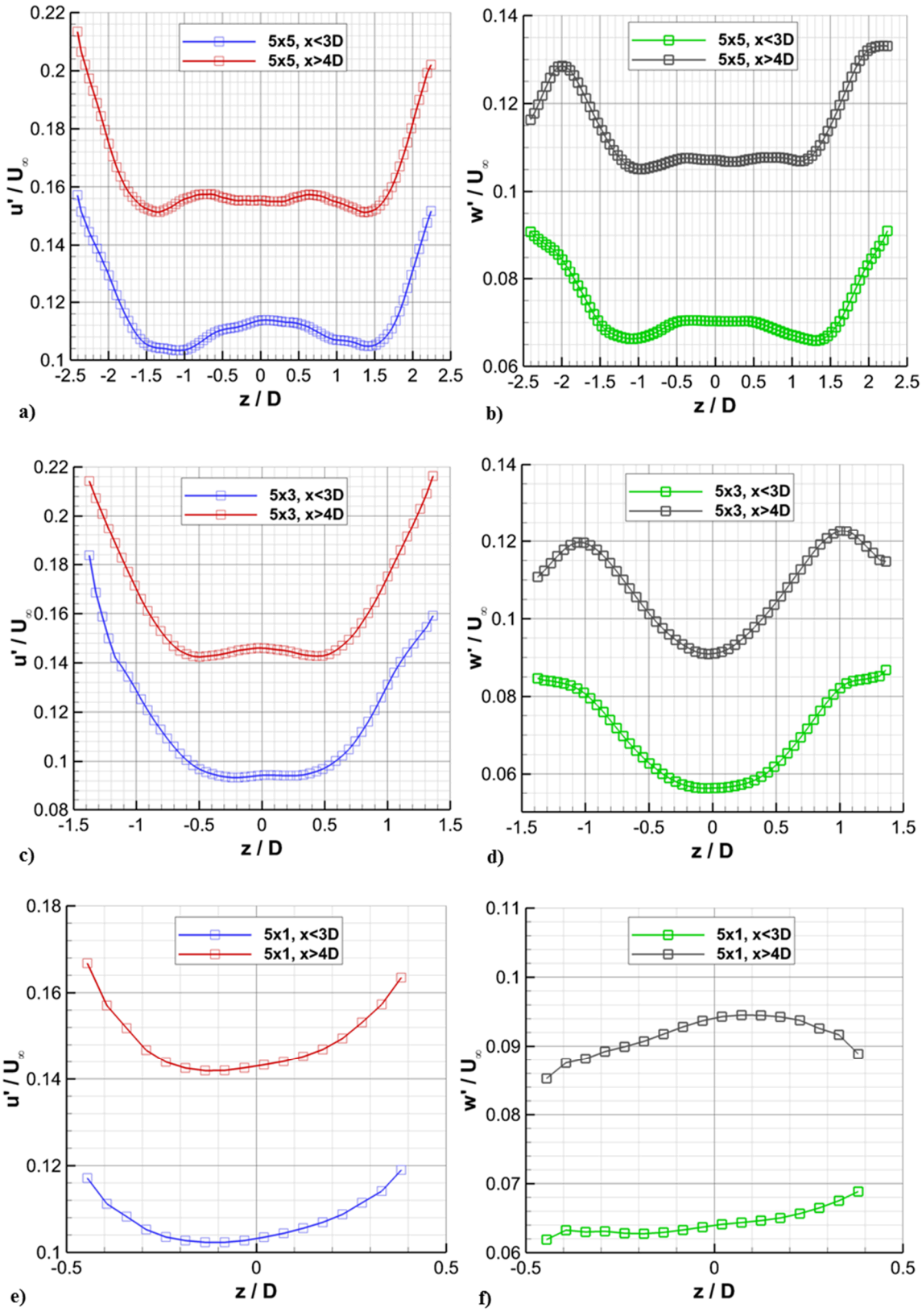

Fig. 7 Turbulence intensity profiles across the cavity span: a) u'/U_∞ (5 × 5), b) w'/U_∞ (5 × 5), c) u'/U_∞ (5 × 3), d) w'/U_∞ (5 × 3), e) u'/U_∞ (5 × 1), and f) w'/U_∞ (5 × 1).

In the upstream portion of the 5 × 5 cavity ($x < 3D$), both the streamwise (Fig. 7a) and spanwise (Fig. 7b) turbulence levels are maximum near the sidewalls with a single local maximum occurring at $z = 0$. As the aft wall is approached ($x > 4$D), the turbulence profiles gain undulations with local maxima occurring near $z = \pm 0.75D$ and local minima near $z = 0$. Moving to the 5 × 3 geometry, both the streamwise (Fig. 7c) and spanwise (Fig. 7d) turbulence profiles become simpler. The upstream profiles decrease monotonically until the spanwise center is reached, whereas the downstream profiles begin to show additional oscillation as the effects of spillage move inboard. In the case of the 5 × 1 cavity, the streamwise profiles (Fig. 7e) decrease monotonically as $z = 0$ is approached. In the spanwise profiles (Fig. 7f), only slight variation is observed in the upstream portion of the cavity ($x < 3D$). The downstream profile shows a trend opposite to all the others with turbulence being maximum near the spanwise center. Overall, the turbulence levels are much more constant across the width of the narrowest cavity.

Inspection of the turbulence contour plots suggests a qualitatively similar behavior to occur near the sidewalls in the 5 × 5 and 5 × 3 cavities. This is perhaps because the wider cavities have enough space to accommodate a counter rotating vortex pair centered at $z = 0$. The similarity of the wider cavities near the spanwise walls is quantified further in Fig. 8, where the abscissa has been transformed to begin at $z = W$. With this transformation, the 5 × 5 and 5 × 3 profiles have similar shape upstream (Fig. 8a) and are in good agreement downstream (Fig. 8b).

Like the mean velocity fields, the turbulence distributions demonstrate increasing complexity and periodicity as the cavity width is increased. It is unknown how these spanwise variations may influence the resonance patterns with the cavity. In the following, the TR-PIV data allow individual modal distributions across the span to be investigated.

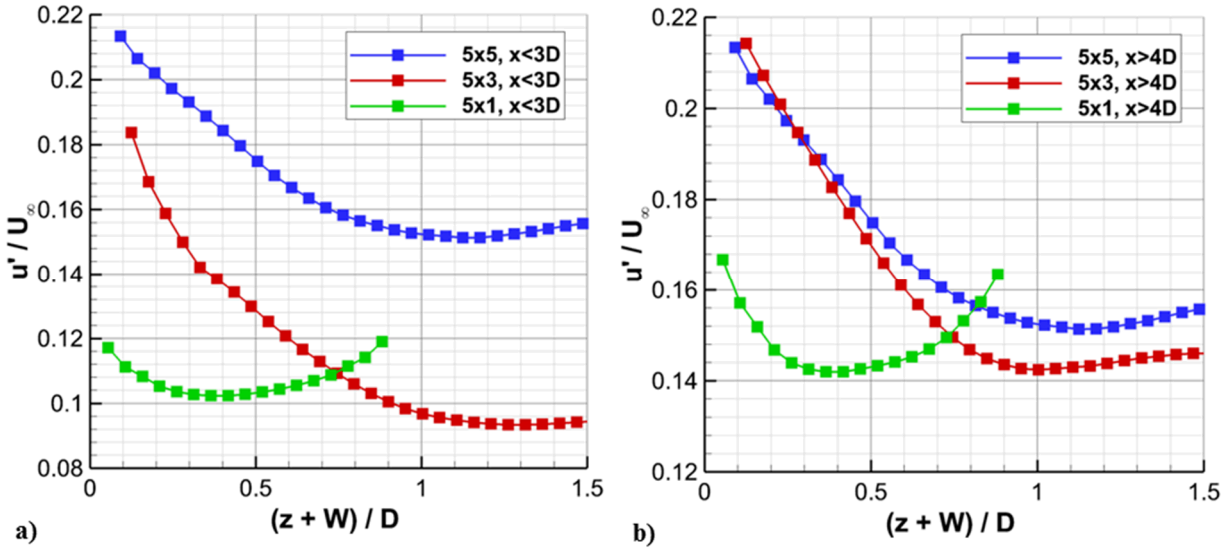

Fig. 8 Spanwise profiles of streamwise turbulence intensity beginning at $z = W$: upstream values averaged over all $x < 3D$, and b) downstream profiles averaged over $x > 4D$.

C. Spatial Distributions of Velocity PSD Modal Amplitude (Modal Velocities)

PSD amplitude distributions of streamwise velocity at frequencies corresponding to cavity modes one through three (i.e. $PSD_u(f_m)$) are shown in Fig. 9. The contours display the square root of PSD amplitude as to maintain units of normalized velocity. The contour scales are held constant at a given mode for each of the three cavity widths. Similarly, spanwise modal velocities at each cavity mode and aspect ratio are presented in Fig. 10.

Inspection of the streamwise (Fig. 9a – Fig. 9c) and spanwise (Fig. 10a –Fig. 10c) mode one velocities suggests mode one to be concentrated near the spanwise walls in the 5 × 5 and 5 × 3 cavities. Importantly, however, modal velocities alone are not an indicator of strong resonance. For example, previous measurements in the spanwise center plane (i.e. the $x - y$ plane) have shown that turbulent fluctuations can overwhelm resonance fluctuations particularly at mode one [24, 25]. This effect was observed to become more pronounced with increasing streamwise distance. Thus, it is important to evaluate PSD spectra at locations of interest. Along these lines, streamwise and spanwise velocity PSDs at a fixed point are shown in Fig. 11. The location of the point PSDs corresponds to the star symbol near the spanwise edge as denoted in Fig. 9 and Fig. 10.

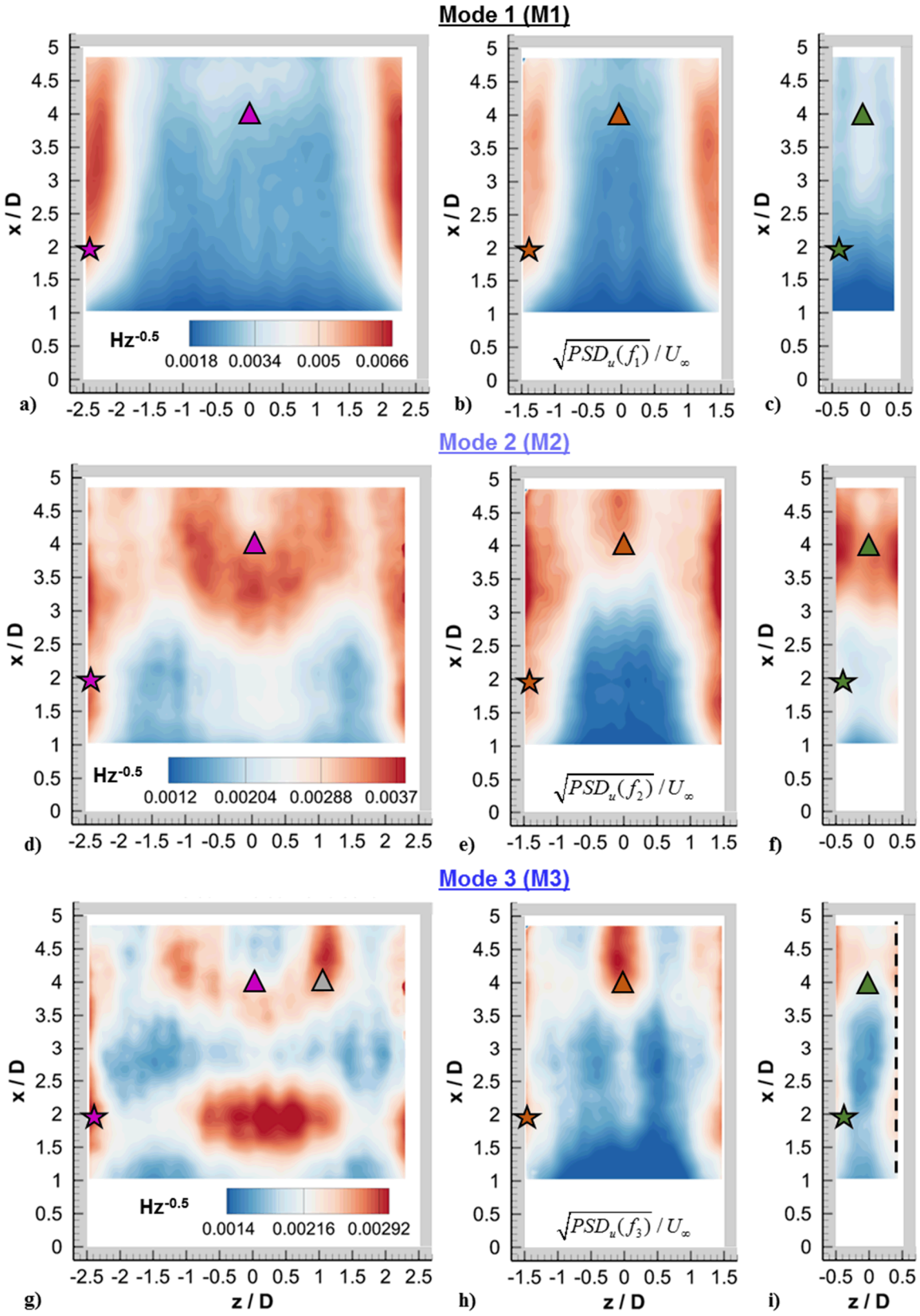

Fig. 9 Streamwise modal velocities: a) Mode 1 (5 × 5), b) Mode 1 (5 × 3), c) Mode 1 (5 × 1), d) Mode 2 (5 × 5), e) Mode 2 (5 × 3), f) Mode 2 (5 × 1), g) Mode 3 (5 × 5), h) Mode 3 (5 × 3), and i) Mode 3 (5 × 1).

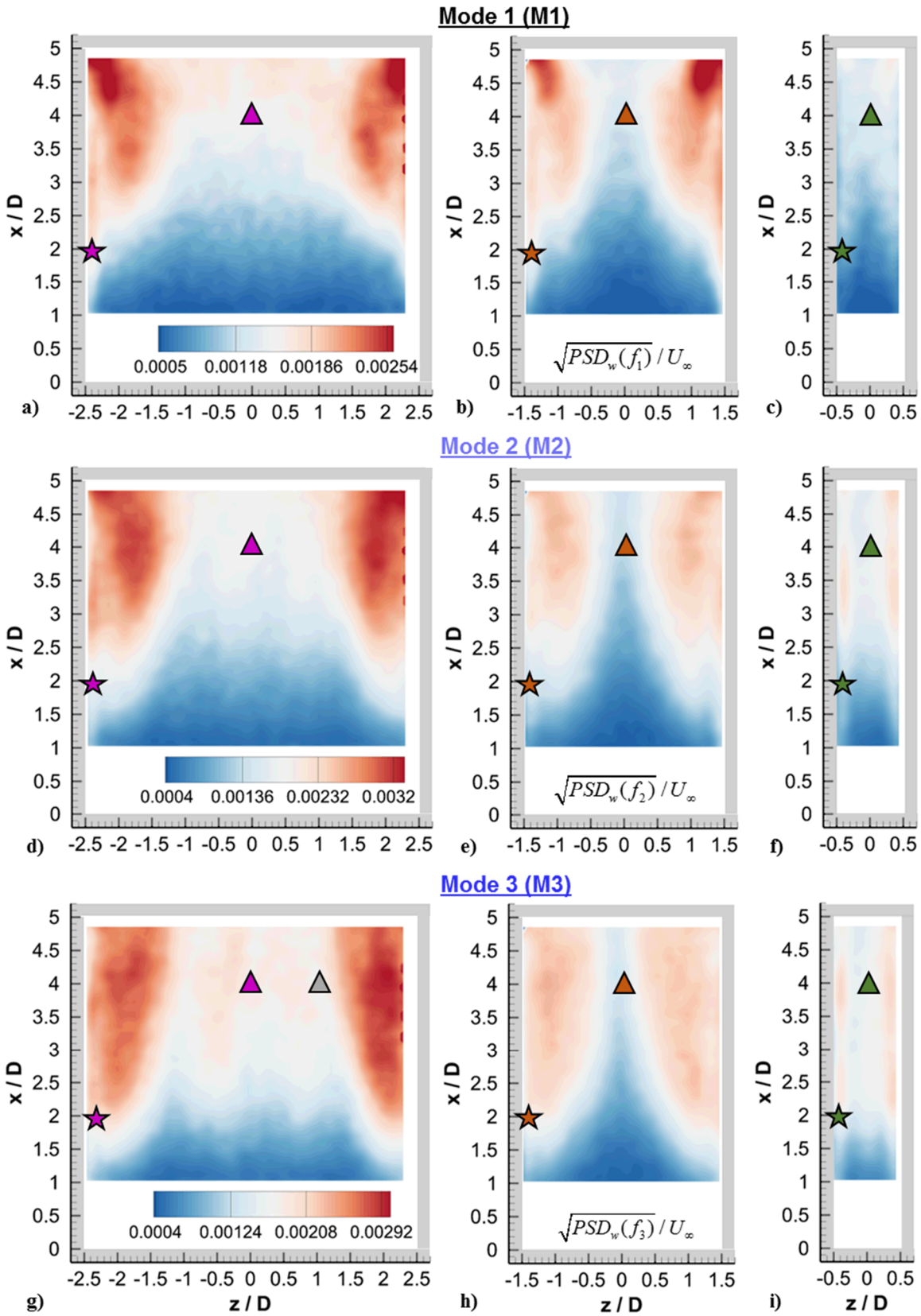

Fig. 10 Spanwise modal velocities: a) Mode 1 (5 × 5), b) Mode 1 (5 × 3), c) Mode 1 (5 × 1), d) Mode 2 (5 × 5), e) Mode 2 (5 × 3), f) Mode 2 (5 × 1), g) Mode 3 (5 × 5), h) Mode 3 (5 × 3), and i) Mode 3 (5 × 1).

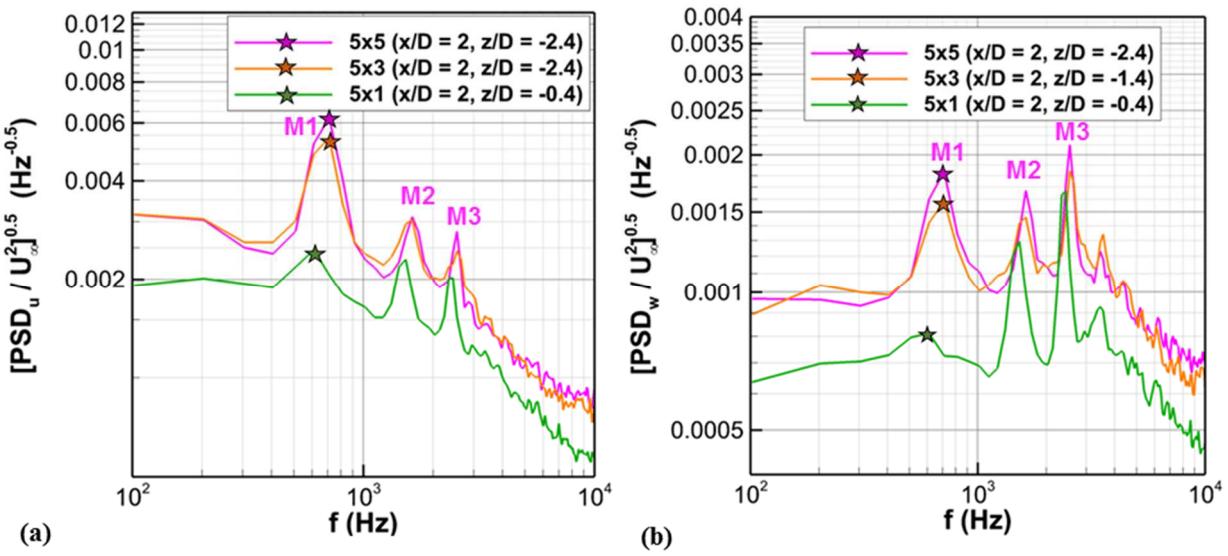

Fig. 11 Point PSDs at x = 2D, z = -2.4D in each cavity configuration: a) streamwise velocity PSD, and b) spanwise velocity PSD. The spectra were acquired at the location denoted with the star symbol in the previous contour plots.

As shown in Fig. 11a, mode one is unequivocally present in the streamwise velocity component near the spanwise edge of the two wider cavities. The amplitude of M1 is a factor of two greater than that at surrounding frequencies. Since the classical (Rossiter) mechanism is based on the propagation of spanwise vorticity, it is quite interesting that M1 is strongest near the spanwise edge, where a large magnitude of streamwise vorticity would be expected. In other words, spillage effects do not appear to diminish mode one here. Rather, they perhaps strengthen it. In comparison, the M1 amplitude in the 5 × 1 spectrum is about 2.5 times lower, consistent with the lower mode one amplitude as registered by the aft wall pressure sensor. Thus, in the present case, it appears strong spillage vortices are related to an elevated mode one amplitude. Perhaps even more interesting, is the large amplitude associated with M1 in the spanwise modal velocity spectra (Fig. 11b). It is not obvious that the resonance mechanism, which is thought to be dominated by the propagation of spanwise aligned vortices, should appear so strongly in the spanwise velocity component. Once again, the 5 × 5 and 5 × 3 cavities show similar behavior as evidenced by comparable M1 amplitudes in the spanwise velocity spectra.

In comparison to mode one, an increased streamwise periodicity is observed at in the streamwise modal velocities of mode two (Fig. 9d – Fig. 9f). This behavior is expected and consistent with a with a decreasing modal wavelength [25]. Local maxima, particularly evident near the sidewalls, occur near x = 1.5D. The fact that streamwise periodicity is observed in the modal velocities near the sidewalls suggests that resonant velocity fluctuations are present above those associated with turbulence. This assessment is confirmed in Fig. 11a with the occurrence of a mode two peak in each of the three cavity geometries. In the mode two spanwise velocities (Fig. 10d – Fig. 10f), the resonance activity moves upstream in comparison to mode one, although a streamwise periodicity is not present. Additionally, prominent M2 peaks occur near the sidewall in the spanwise velocity spectra of each cavity geometry (Fig. 11b).

As the mode number increases to three, a further decrease in streamwise wavelength is observed in Fig. 10g – Fig. 10i. In the upstream portion of the cavity near x = 2D, a spanwise periodicity is also observed in the wider cavities. Once more, the presence of a streamwise wavelength at the sidewalls (i.e. constant z /D) suggests these regions to be highly influenced by resonance fluctuations and not just turbulence. The prominent mode three peaks in Fig. 11a confirm this statement. The spanwise modal velocity distributions look like those at mode two, except that the resonance activity moves upstream with mode number. Prominent peaks in the spanwise velocity spectra (Fig. 11) at mode three continue to suggest a highly three-dimensional resonance process.

Variations in the modal velocities occur across the spanwise direction of the cavity. Except for mode one in the 5 × 5 geometry, the modal activity increases near the sidewalls. As the aft wall is approached, the wider cavities appear to exhibit increased spanwise periodicity, particularly in the streamwise modal velocities of mode two (Fig. 9d, Fig. 9e) and mode three (Fig. 9g, Fig. 9h).

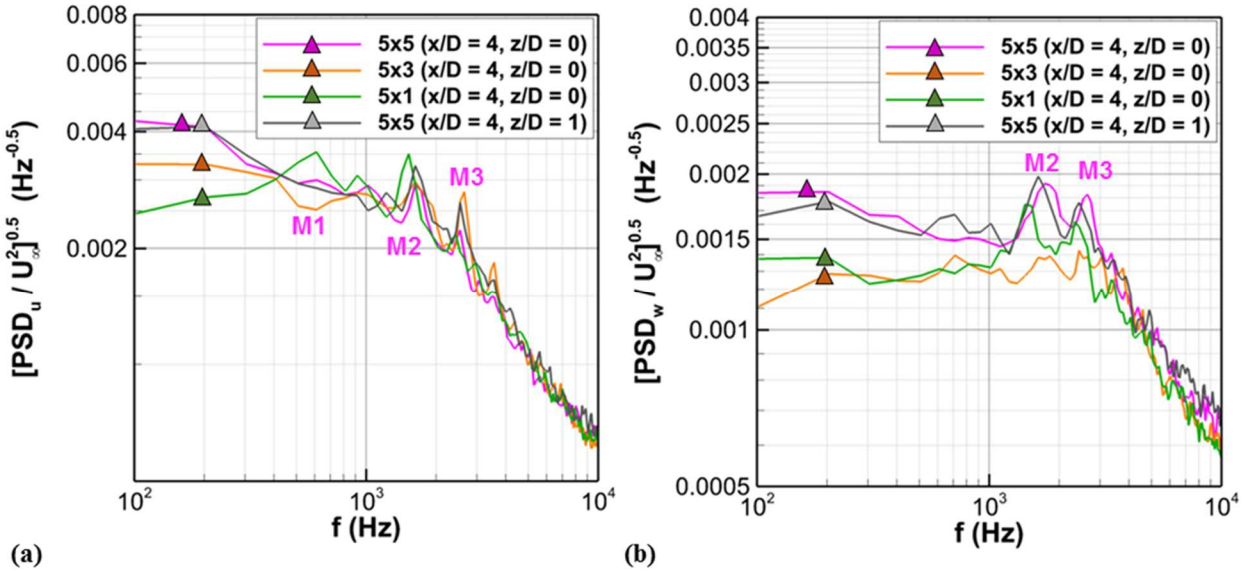

Fig. 12 Point PSDs near the aft end of each cavity configuration: a) streamwise velocity PSD, and b) spanwise velocity PSD. The spectra were acquired at the locations denoted with the triangular symbol in the previous contour plots.

Point PSDs corresponding to $x = 4D$, $z = 0$ are shown in Fig. 12. In the streamwise velocity spectra (Fig. 12a), modes two and three are measurable above the increased turbulence levels (Fig. 5). Mode one, on the other hand, does not rise above surrounding broadband fluctuation levels except in the instance of the 5 × 1 cavity. Importantly, although not shown, M1 peaks are observed in each cavity geometry in analogous spectra obtained at $x = 4D$, $z = -2.4D$.

Interpretation of the spanwise spectra of Fig. 12b is more nuanced. At $z = 0$, peaks at modes two and three occur in the 5 × 5 and 5 × 1 spectra. Slight peaks are also present in the 5 × 3 spectrum, although at levels much more comparable to surrounding frequencies. Collectively, these observations indicate that broadband fluctuations play a larger role near the aft portion of the cavity particularly at mode one and in the spanwise distributions.

The influence of the sidewalls can be investigated further with evaluation of point PSDs at additional locations. A local maximum is present at $x = 4D$, $z = 0$ in the 5 × 3 streamwise velocity distribution of mode three (Fig. 9f). In contrast, the corresponding 5 × 5 distribution (Fig. 9g) exhibits a local minimum at this location. The center of the 5 × 3 cavity is $1.5D$ away from the sidewalls. Point PSDs in the 5 × 5 cavity, calculated at $z = 1D$ ($1.5D$ away from the sidewall), are also shown in Fig. 12. At this location, M3 is more prominent in the streamwise spectrum (Fig. 12a) with an amplitude comparable to that in 5 × 3 cavity. Therefore, like the turbulence fields, the 5 × 5 and 5 × 3 cavity can show similar modal behavior when the spanwise coordinate originates at the sidewall.

Inspection of the modal velocity distributions in Fig. 9 and Fig. 10 suggests the presence of universal trends for a given cavity aspect ratio. In other words, at a given cavity geometry, some similarities in the spanwise variation of modal velocity distributions are apparent independent of mode number. This observation is quantified using spanwise profiles of modal velocity. Like the previous turbulence profiles, the modal velocities were averaged over the streamwise direction to produce upstream ($x < 3D$) and downstream ($x > 4D$) profiles. This analysis was performed for modes one through three of each cavity configuration on the streamwise modal velocity (Fig. 13) and the spanwise modal velocity (Fig. 14).

Profiles of streamwise modal velocity across the span of the 5 × 5 cavity are presented in Fig. 13a and Fig. 13b. In the upstream portion of the cavity (Fig. 13a), the profiles corresponding to mode 2 (M2) and mode 3 (M3) are quite similar. Like the profile of streamwise turbulence intensity in Fig. 7a, the modal fluctuations exhibit local maxima near the sidewalls and at the spanwise center. In comparison, the mode one (M1) profile has larger velocities near the sidewalls, but a local maximum near $z = 0$ is still apparent. The downstream profiles (Fig. 13b) corresponding to modes two and three also have similar shape. (The mode one profile is unlike modes two and three and is omitted for clarity.) Once again, like the turbulence plot in Fig. 7b, the spanwise wavelength decreases at the more aft location.

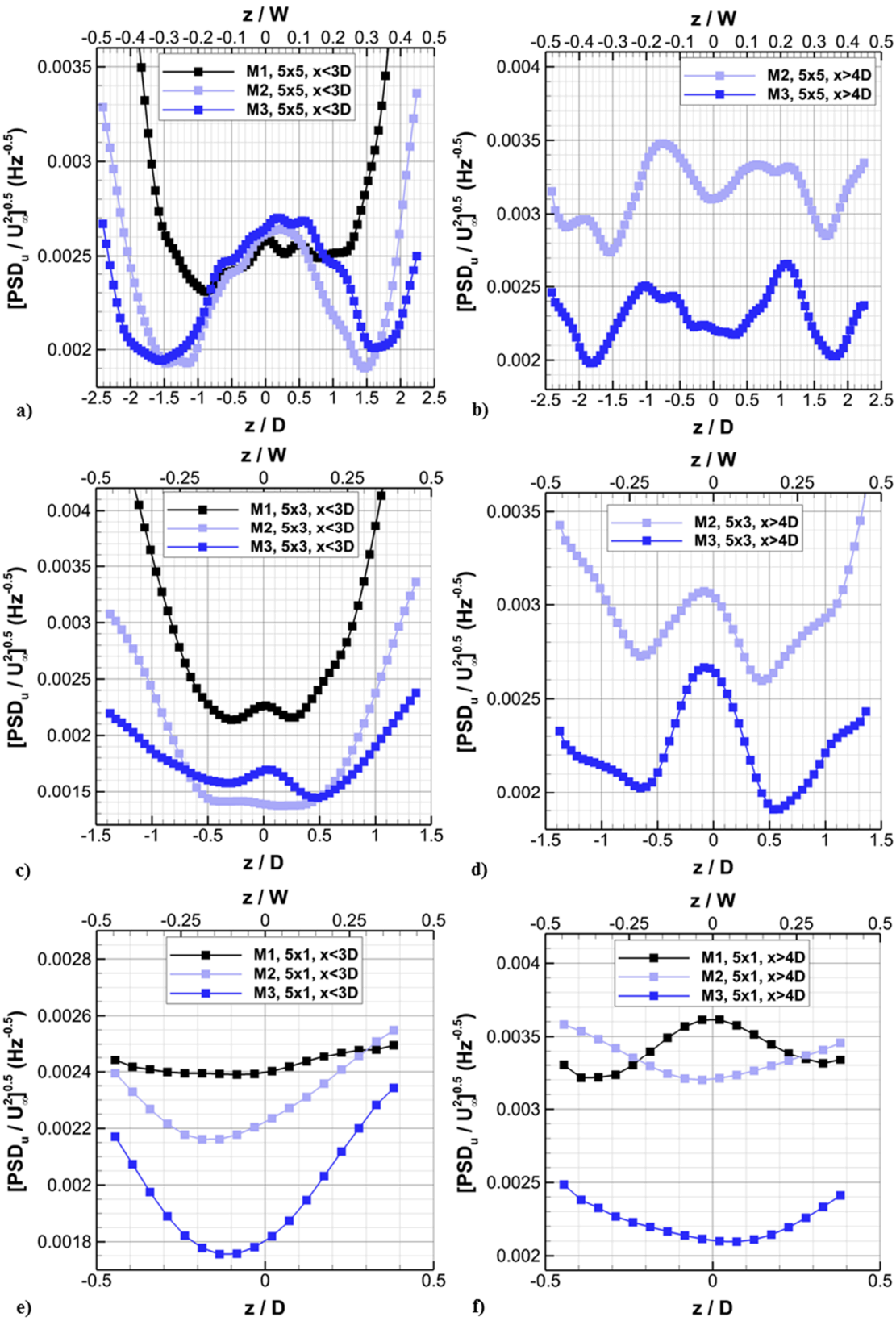

Fig. 13 Streamwise modal velocity profiles across the cavity span: a) 5 × 5 upstream (x < 3*D*), b) 5 × 5 downstream (x > 4*D*), c) 5 × 3 upstream, d) 5 × 3 downstream, e) 5 × 1 upstream, and f) 5 × 1 downstream.

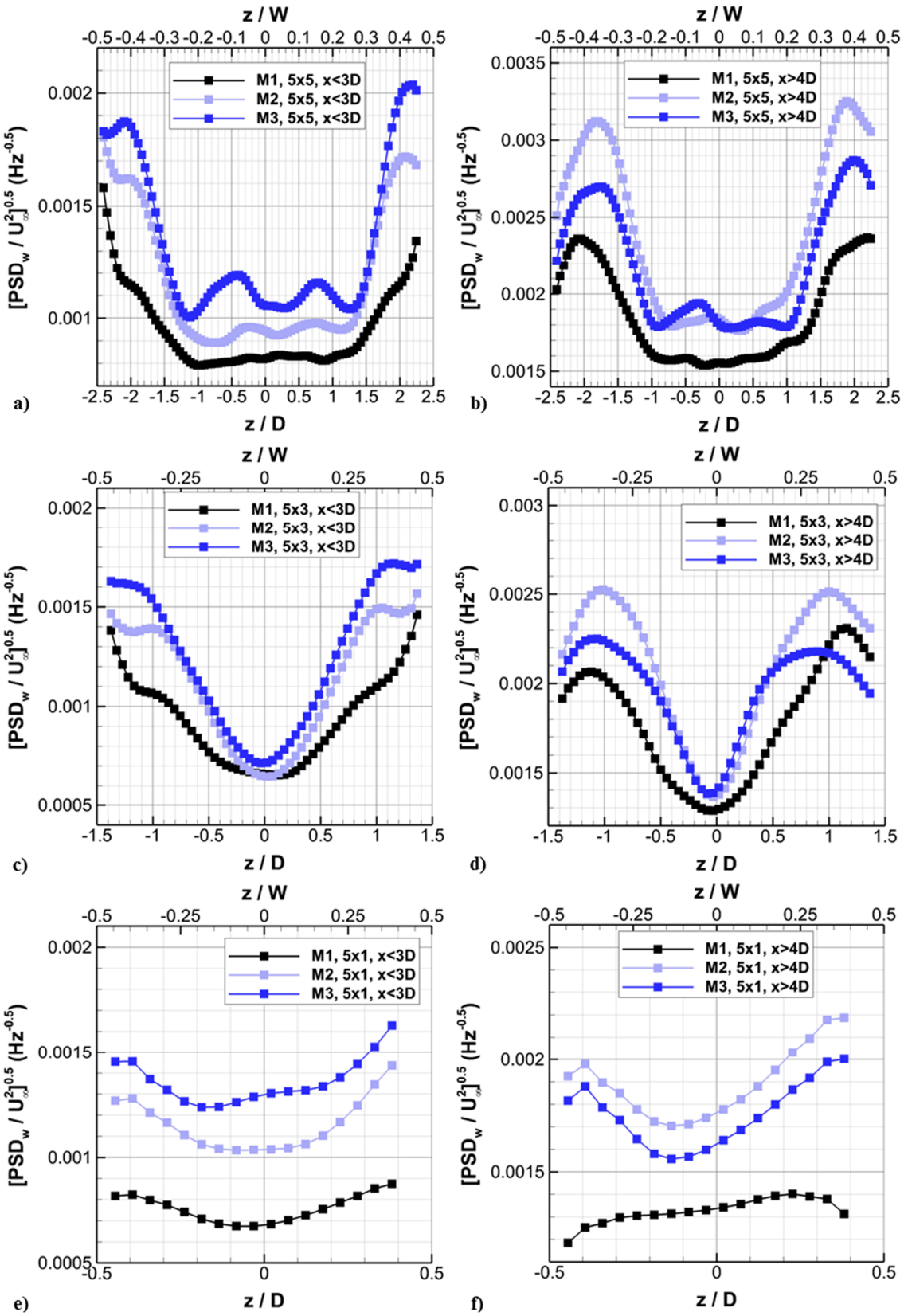

Fig. 14 Spanwise modal velocity profiles across the cavity span: a) 5 × 5 upstream (x < 3*D*), b) 5 × 5 downstream (x > 4*D*), c) 5 × 3 upstream, d) 5 × 3 downstream, e) 5 × 1 upstream, and f) 5 × 1 downstream.

The profiles of streamwise modal velocity across the span of the 5 × 3 cavity exhibit some similar trends. Upstream (Fig. 13c), the profiles have similar shape either exhibiting a minimum at the spanwise center (M2) or a small peak (M1 and M3). In comparison, the downstream profiles (Fig. 13d) demonstrate increased variation across the span with a prominent local maximum occurring at the spanwise center. A local, though less prominent, maximum is also observed in the $x > 4D$ streamwise turbulence intensity profile of Fig. 7b. In comparison to the 5 × 5 profiles there is less variation across the span of the cavity.

Decreasing the width to D results in further simplification of the streamwise modal velocity profiles. Both upstream (Fig. 13e) and downstream (Fig. 13f), the modal velocities show less variation across the span than those in the wider cavities. Each profile contains a local minimum near the spanwise center except for the downstream M1 profile, which demonstrates the opposite behavior. Furthermore, the shapes of the modal velocity profiles are similar to the turbulence profiles shown in Fig. 7c.

A strong dependence on cavity geometry is also observed in the spanwise modal velocity profiles of Fig. 14. In each profile, the spanwise modal velocity is maximum near the sidewall except the downstream profile of mode one (Fig. 14f). At a given cavity geometry, the spanwise modal velocities increase with streamwise distance. The shapes of the spanwise modal velocity profiles are fairly constant at a given cavity geometry and streamwise location. Moreover, the periodicity of the profiles decreases as the cavity narrows. Finally, for the most part, the profiles are similar in shape to the spanwise turbulence intensity plots of Fig. 14.

In summary, the spanwise variation of modal resonance fluctuations is largely dependent on cavity aspect ratio.

D. TR-PSP

An example of TR-PSP results corresponding to the third mode of the 5 × 1 cavity is shown in Fig. 15a. The PSP distribution was acquired on the floor of the cavity, which is denoted by the solid rectangle. The mode three pressure distribution on the wind tunnel floor ($y = 0$) surrounding the cavity is additionally displayed. Like previous results in the 5 × 5 geometry [25], three minima occur along the floor of the 5 × 1 cavity. Outside of the cavity, a similar periodicity is observed. The spillage pattern is swept downstream away from the cavity side walls owing to the surrounding higher speed fluid. The peaks in mode three pressure fluctuations are quite pronounced along the top of the spanwise walls adjacent to the cavity. In fact, at most streamwise locations, the peak modal pressures occur along the wind tunnel wall as opposed to on the cavity floor. Similar observations were made in each cavity geometry at each cavity mode frequency. This illustration of prominent spillage fluctuations outside of the cavity shows why it is necessary to break up acoustic modes associated with interference of the wind tunnel walls using sidewall acoustic dampeners.

The streamwise periodicity is highlighted further in fig. 15b, where the modal pressure fluctuations along x, at $y = 0$, $z = 0.6D$ (i.e. the dashed line in Fig. 15a) are shown. Additionally, the mode three streamwise velocities obtained along the dashed line annotated in Fig. 9i are given. Like previous work [25], the modal velocity and pressure waveforms are 180 degrees out of phase suggesting acoustical mechanisms analogous to a standing wave. Thus, strong modal acoustical signatures are clearly evident in both the pressure and velocity fields near the spanwise edges of the cavity.

IV. Summary and Future Work

The resonance characteristics in the planform plane just above the cavity lip line were studied for three different cavity aspect ratios using TR-PIV with a pulse-burst laser. The experiments were conducted at a freestream Mach number 0.94, where strong resonance was observed at the first three cavity mode frequencies. Three geometries were tested where the length × width ratio was $5D \times 5D$, $5D \times 3D$, and $5D \times 1D$.

The current work extends upon that of Beresh et al. where the effects of finite span on the mean flow and turbulence distributions have been discovered for transonic [30] and supersonic [31] Mach numbers in the same cavity geometries. Like these previous studies, the present work showed the cavity sidewalls to have a substantial influence on the mean and turbulence fields. The most significant spanwise alteration of these statistical properties was observed to occur in the two widest cavities, namely the 5 × 5 and 5 × 3 geometries. In these configurations, the presence of inflow along the spanwise sidewalls leads to spillage vortices and the generation of increased turbulence levels.

The use of TR-PIV allowed for resonance distributions across the cavity span to be characterized. This was achieved primarily by plotting the distribution of velocity PSD amplitude at the modal frequencies. These modal velocity fields were generated using both the streamwise and spanwise components of velocity. In each mode of each cavity configuration, strong resonance fluctuations appear near the sidewalls. In other words, despite increased

turbulence levels in the spillage regions, modal activity is still quite strong. As a result, a streamwise periodicity is observed in the streamwise modal velocity distributions near the sidewalls. Similarly, TR-PSP data on the wind tunnel floor adjacent to the cavity sidewall showed strong pressure fluctuation to occur in the spillage regions. Like previous work, the modal pressures were approximately 180 degrees out of phase with the modal velocities.

Interestingly, prominent peaks at the modal frequencies also occur in the spanwise modal velocity fields near the sidewalls. This suggests a more three-dimensional resonance mechanism than that in the classical Rossiter interpretation.

Obvious variations in resonance fluctuations (modal velocities) were observed across the span of the cavity. The characteristics and periodicity of these variations was found to be a strong function of cavity geometry. Put otherwise, common trends across modes one through three were observed at a fixed cavity geometry. In many ways, the spanwise variations in modal velocity were akin to those observed in the turbulence fields. These observations held true in both the streamwise and spanwise modal velocity fields.

Despite the aforementioned commonalities, significant differences between the two wider cavities and the narrowest (5 × 1) cavity were observed. In addition to having significantly lower turbulence levels associated with spillage, the 5 × 1 configuration was found to substantially decreased fluctuations in mode one velocities in comparison to the 5 × 3 and 5 × 5 cavities. Likewise, the mode one amplitude in the 5 × 1 cavity, as measured using pressure sensors and TR-PSP, was also significantly diminished in comparison to that in the two wider cavities. These observations suggest that the spillage regions may play a role in the prominence of mode one amplitudes.

Future work will further utilize the TR-PSP data obtained at each cavity configuration beyond the single example presented here. Moreover, bandpass-filtered modal velocity fields will be studied to gain further understanding of the three-dimensionality present in the resonance distributions.

Altogether, this study presents conclusive evidence that the sidewall effects in finite span cavities play a key role on the three-dimensional distribution of resonance fluctuations. Such implications are important to understanding FSI in aircraft bay flows as well store separation.

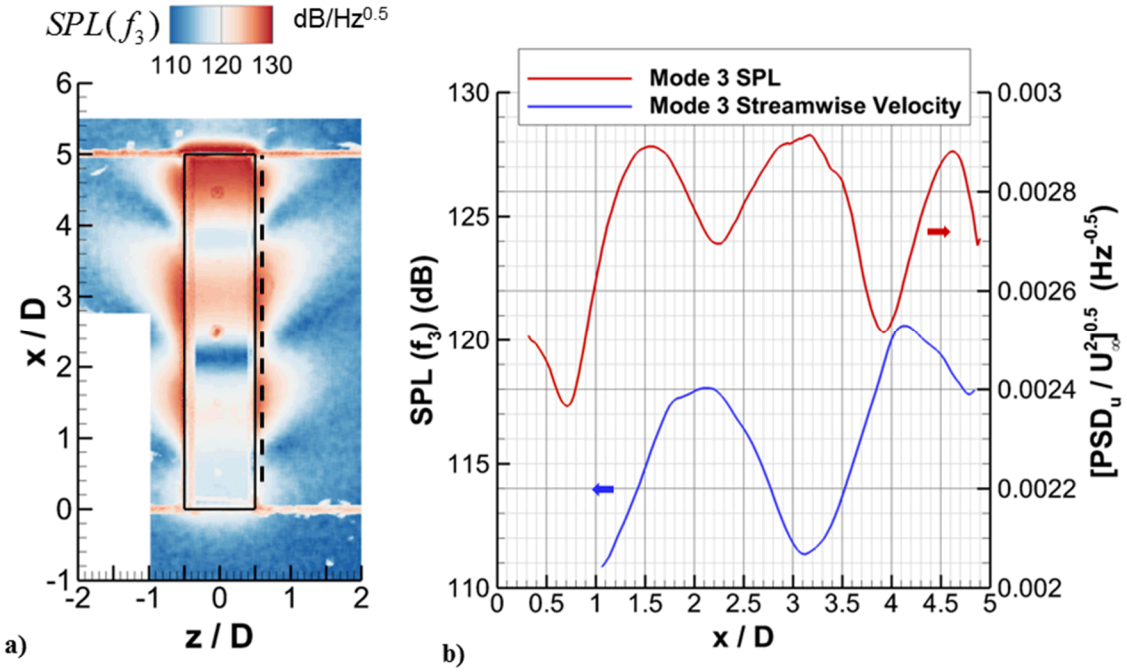

Fig. 15 TR-PSP: a) distribution of SPL(f_3) along the floor (y = -D) of the 5 × 1 cavity along with the modal pressure field measured on the wind tunnel floor (y = 0), and b) comparison of the mode 3 SPL distribution along the wind tunnel floor in in the spillage region (z = 0.6D) compared to the streamwise distribution of mode 3 streamwise velocity measured near the side wall at (z = 0.4D).

References

[1] Rockwell, D., and Naudascher, E., "Self-sustained oscillations of impinging free shear layers," *Annual Review of Fluid Mechanics*, Vol. 11, 1979, pp. 67-94.

[2] Rockwell, D., and Naudascher, E., "Review-Self Sustaining Oscillations of Flow Past Cavities," *Journal of Fluids Engineering*, Vol. 100, 1978, pp. 152-165.
[3] Rowley, C. W., and Williams, D. R., "Dynamics and Control of High-Reynolds-Number Flow over Open Cavities," *Annual Review of Fluid Mechanics*, Vol. 38, 2006, pp. 251-276.
[4] Cattafesta, L. N., Song, Q., Williams D. R., Rowley C. W., and Alvi, F. S., "Active control of flow-induced cavity oscillations," *Progress in Aerospace Sciences*, Vol. 44, 2008, pp. 479-502.
[5] Rossiter, J. E., "Wind-Tunnel Experiments on the Flow Over Rectangular Cavities at Subsonic and Transonic Speeds," Aeronautical Research Council Reports and Memoranda, October 1964.
[6] Tracy, M. B., and Plentovich, E. B., "Cavity Unsteady-Pressure Measurements at Subsonic and Transonic Speeds," NASA Technical Paper 3669, December 1997.
[7] Wagner, J. L., Casper, K. M., Beresh, S. J., Hunter, P. S., Spillers, R. W., Henfling, J. F., and Mayes, R. L., "Fluid-structure interactions in compressible cavity flows," *Physics of Fluids*, Vol. 26, No. 6, pp.066102.
[8] Barone, M., and Arunajatesan, S., "Pressure Loadings in a Rectangular Cavities with and Without a Captive Store, *Journal of Aircraft*, Vol. 53. No. 4, pp. 982-991.
[9] Wagner, J. L., Casper, K. M., Beresh, S. J., Hunter, P. S., Spillers, R. W., and Henfling, J. F., "Response of a Store with Tunable Natural Frequencies in Compressible Cavity Flow," *AIAA Journal*, Vol. 54, No. 8, 2016, pp. 2351-2360.
[10] Murray, N. E., Jansen, B. J., Gui, L., Seiner, J. M., and Birbeck, R., "Measurements of Store Separation Dynamics," AIAA Paper 2009-105.
[11] Ahuja, K. K. and Mendoza, J., "Effects of Cavity Dimensions, Boundary Layer, and Temperature on Cavity Noise with Emphasis on Benchmark Data to Validate Computational Aeroacoustic Codes," Contractor Report 4653, NASA, 1995.
[12] Disimile, P. J., Toy, N., and Savory, E., "Effect of Planform Aspect Ratio on Flow Oscillations in Rectangular Cavities," *Journal of Fluids Engineering*, Vol. 122, No. 1, 2000, pp. 32-38.
[13] Woo, C., Jim, J., and Lee, K., "Three-Dimensional Effects of Supersonic Cavity Flow due to the Variation of Cavity Aspect and Width Ratios," *Journal of Mechanical Science and Technology*, Vol. 22, No. 3, 2008, pp. 590-598.
[14] Beresh, S. J., Wagner, J. L., and Casper, K. M., "Compressibility Effects in the Shear Layer over a Rectangular Cavity," *Journal of Fluid Mechanics*, Vol. 808, 2016, pp.116-152.
[15] Casper, K. M., Wagner, J. L., Beresh, S. J., Henfling, J. F., Spillers, R. W., & Pruett, B. O., "Complex Geometry Effects on Cavity Resonance," *AIAA Journal*, Vol. 54, No. 1, 2015, pp. 320-330.
[16] Ukeiley, L., Sheehan, M., Coiffet, F., Alvi, F., Arunajatesan, S., and Jansen, B., "Control of pressure loads in geometrically complex cavities," *Journal of Aircraft*, Vol. 45, No. 3, 2008, pp.1014-1024.
[17] DeMauro, E. P., Casper, K. M., Beresh, S. J., Wagner, J. L., Henfling, J. F., and Spillers, R. W., "Study of the Flow within Finite-Span Complex Cavities using Particle Image Velocimetry and Pressure Sensitive Paint," AIAA Paper 2017-1474.
[18] Kegerise, M. A., "An Experimental Investigation of Flow Induced Cavity Oscillations," Ph.D. Thesis, Department of Mechanical Engineering, Syracuse University, New York, USA, 1999.
[19] Kegerise, M. A., Spina, E. F., Garg, S., Cattafesta, L. N., "Mode-Switching and Nonlinear Effects in Compressible Flow Over a Cavity," *Physics of Fluids*, Vol. 16, No. 3, 2005, pp. 678-687.
[20] Larchevêque, L., Sagaut, P., Lê, T. P., and Compte, P., "Large-eddy simulation of a compressible flow in a three-dimensional open cavity at high Reynolds number," *Journal of Fluid Mechanics*, Vol. 516, 2004, pp. 265-301.
[21] Delprat, N., "Rossiter's formula: A simple spectral model for a complex amplitude modulation process?," *Physics of Fluids*, Vol. 18, No. 7, 2006, pp. 309-339..
[22] Guéniat, F., Pastur, L., Lusseyran, F., "Investigating mode competition and three-dimensional features from two-dimensional velocity fields in an open cavity flow by modal decompositions," *Physics of Fluids*, Vol. 26, No. 8, 2014 ,pp. 085101.
[23] Casper, K. M., Wagner, J. L., Beresh, S. J., Henfling, J. F., Spillers, R. W., and Dechant, L. J., "Spatial Distribution of Pressure Resonance in Compressible Cavity Flow," AIAA Paper 2017-1474, also under review in *Journal of Fluid Mechanics*.
[24] Beresh, S. J., Wagner, J. L., DeMauro, E. P., Henfling, J. F., and Spillers, R. W, "Spatial distribution of resonance in the velocity field for transonic flow over a rectangular cavity," *AIAA Journal*, Vol. 55, No. 12, 2017, pp. 4203-4218.
[25] Wagner, J. L., Casper, K. M., Beresh, S. J., DeMauro, E. P., and Arunajatesan, S., "Resonance Dynamics in Compressible Cavity Flows using Time-Resolved Velocity and Surface Pressure Fields," *Journal of Fluid Mechanics*, Vol. 830, pp. 494-527.
[26] George, B., Ukeiley, L., Cattafesta, L. N., and Taira, K., "Control of Three-Dimensional Cavity Flow using Leading-Edge Slot Blowing," AIAA Paper 2015-1059.
[27] Sun, Y., Zhang, Y., Taira, K., Cattafesta, L. N., George, B., and Ukeiley, L. S., "Width and Sidewall Effects on High-Speed Cavity Flows," AIAA Paper 2016-1343.
[28] Dudley, J. G. and Ukeiley, L., "Detached Eddy Simulation of a Supersonic Cavity Flow with and without Passive Flow Control,"AIAA Paper 2011-3844.
[29] Crook, S. D., Lau, T. C. W., and Kelso, R. M., "Three-dimensional Flow within Shallow, Narrow Cavities," *Journal of Fluid Mechanics*, Vol. 735, 2013, pp. 587-612.
[30] Beresh, S. J., Wagner, J. L., Pruett, B. O., Henfling, J. F., and Spillers, R. W., "Supersonic Flow over a Finite-Width Rectangular Cavity," *AIAA Journal*, Vol. 53, No. 2, 2014, pp. 296-310.
[31] Beresh, S. J., Wagner, J. L., Henfling, J. F., Spillers, R. W., and Pruett, B. O., "Width Effects in Transonic Flow over a Rectangular Cavity," *AIAA Journal*, Vol. 53, No. 12, 2015, pp. 3831-3835.
[32] Arunajatesan, S., Barone, M. F., Wagner, J. L., Casper, K. M., and Beresh, S. J., "Joint experimental/computational investigation into the effects of finite width on transonic cavity flow," AIAA Paper 2014-3027.

[33] Song, Q., Closed-Loop Control of Flow-Induced Cavity Oscillations, Ph.D. Thesis, Department of Mechanical and Aerospace Engineering, University of Florida, Gainesville, USA, 2008.
[34] Murray, N. E., Sallstrom, E., and Ukeiley, L., "Properties of Subsonic Open Cavity Flow Fields," *Physics of Fluids*, Vol. 21, No. 9, 2009, pp. 095103.
[35] Wagner, J. L., Casper, K. M., Beresh, S. J., Pruett, B. O., Spillers R. W., and Henfling, J. F., "Mitigation of Wind Tunnel Wall Interactions in Subsonic Cavity Flows," *Experiments in Fluids*, Vol. 56, No. 3, 2015, pp. 59.
[36] Samimy, M., and Lele, S. K., "Motion of Particles with Inertia in a Compressible Free Shear Layer," *Physics of Fluids A*, Vol. 3, No. 8, 1991, pp. 1915-1923.
[37] Slipchenko, M. N., Miller, J. D., Roy, S., Gord, J. R., Danczyk, S. A., and Meyer, T. R., "Quasi-Continuous Burst-Mode Laser for High-Speed Planar Imaging," *Optics Letters*, Vol. 37, No. 8, 2012, pp. 1346-1348.
[38] Slipchenko, M. N., Miller, J. D., Roy, S., Gord, J. R., and Meyer, T. R., "All-Diode-Pumped Quasi-Continuous Burst-Mode Laser for Extended High-Speed Planar Imaging," *Optics Express*, Vol. 21, No. 1, 2013, pp. 681-689.
[39] Beresh, S. J., Kearney, S. P., Wagner, J. L., Guildenbecher, D. R., Henfling, J. F., Spillers, R. W., Pruett, B. O., Jiang, N., Slipchenko, M., Mance, J., and Roy, S., "Pulse-Burst PIV in a High-Speed Wind Tunnel," *Measurement Science and Technology*, Vol. 26, No. 9, 2015, 095305.
[40] Heller, H. H., and Bliss, D. B., "The Physical Mechanism of Flow Induced Pressure Fluctuations in Cavities and Concepts for Suppression," AIAA Paper 75-491.
[41] Wagner, J. L., Casper, K. M., Beresh, Lynch, K. P., S. J., DeMauro, E. P., and Arunajatesan, S., "Preliminary Investigation of Sidewall Effects on Cavity Resonance Dynamics using Time-Resolved Particle Image Velocimetry and Pressure Sensitive Paint," AIAA Paper 2017-3126.